

Influence of the Titanium Carbide Reinforcing Phase Content on Surface Geometric Structure Parameters of H13 Steel-Based Composite Materials Obtained by Selective Laser Melting

Emilia Bachtiaik-Radka¹, Marta Beata Krawczyk^{2*}

¹ Department of Production Management, West Pomeranian University of Technology in Szczecin, Piastow Av. 19, 70-310 Szczecin, Poland

² Department of Manufacturing Engineering, West Pomeranian University of Technology in Szczecin, Piastow Av. 19, 70-310 Szczecin, Poland

* Corresponding author's e-mail: wimim.ktw@zut.edu.pl

ABSTRACT

The paper presents the results of research on the surface geometric structure (SGS) of objects made of H13 tool steel reinforced with titanium carbide (TiC) nanoparticles with a concentration between 2.5 and 15% vol., manufactured using the additive manufacturing method (AM) – selective laser melting (SLM). The variable parameters were the percentage of the reinforcing phase and the spatial orientation of the analysed surfaces, while the SLM process parameters were constant. The altitudinal and spatial SGS parameters obtained for the studied samples and surfaces are summarised and compared. The results showed a strong influence of the reinforcing phase content on the values of the surface roughness parameters – with the significant deterioration noted for samples with min. 10% TiC vol. The resulting surface quality was better for upward-facing than downward-facing produced at the same angle.

Keywords: additive manufacturing, composites, surface geometry, roughness.

INTRODUCTION

Hot work tool steels are widely used for making forging die heads and extrusion mandrels, and wear is one of the factors causing premature failure of these tools [1–5, 36]. However, high impulsive load and elevated temperature often give rise to wear and thermal fatigue failure in the surfaces of the dies during practical application [6]. It is known that the microstructure and mechanical properties of surfaces show a key role in resistance to wear and thermal fatigue. Therefore, improving the microstructure and mechanical properties of H13 steel is essential to extend its service life. The addition of ceramic particles has been proven to increase the wear resistance and service life of hot work tool steels [5, 8–10]. TiC is an effective reinforcement for steel matrix composites due to its high hardness, stability, and

good wettability [4, 11]. In recent years, many techniques have been presented for the production of composite TiC reinforced that are based on ex-situ for example selective laser melting [8, 9, 12–22], laser cladding [3, 23–25] or sintering [5, 10], and in-situ methods for example casting [26, 27] or laser surface modification methods [11, 28, 29].

Research on composite materials made of H13 steel reinforced with TiC particles has already been conducted. For example, Dadoo et al [1] studied H13/TiC composite coatings produced using a pulsed laser surface alloying technique. In another paper [2], they analysed the effect of process variables on the shape and size of carbide precipitates. Meng et al. in the paper [7] studied the mechanical properties and microstructures of H13 steel processed by bionic laser surface alloying with different fractions of TiC particulates.

However, in the paper [23] Zhang et al. explore the effect of tempering treatment on the microstructure and properties of TiC reinforced H13 steel composites, and provide theoretical support and practical reference for extending the life of H13 steel. The study of the dependence of microstructure and hardness on the proportion of reinforcing phase in H13/TiC composites was also conducted by Chen et al [3]. Kazem et al [4] in their study focused on the effect of pulsed laser method parameters on microhardness and abrasive wear of H13/TiC composite materials. Research on composite coatings obtained by laser cladding technique was conducted by Gu et al [24], who in their work using finite element simulations of nanoindentation determined the critical maximum tensile stress. Henschel et al. in their paper [5] investigated the effect of a reinforcing phase such as 20% TiC addition on the fracture toughness of the hot work AISI H13 tool steel. They noted that for spark plasma sintering, the addition of carbides resulted in reduced fracture toughness, which was attributed to the relatively low density of the test samples. Papers [12, 25, 30] present the results of research on the influence of process parameters on the morphology and properties of steel matrix composite materials reinforced with titanium carbides. It has been shown in these studies that with the right choice of process scenario, materials characterised by different microhardness can be obtained. It can therefore be seen that the strength properties of H13/TiC composite materials have already been investigated. However, all components, especially mating components, must meet surface quality requirements in addition to the relevant mechanical requirements. Thus, Wei et al. [31] discussed the effect of process parameters on the surface quality, microstructure and mechanical properties of AlSi10Mg. They have shown that continuous scan paths with relatively smooth surfaces can be produced in a suitable narrow energy range, thereby reducing the formation of porosity during the SLM process and improving the densification of SLM-produced parts. In [13], Bi et al. investigated the influence of SLM process parameters on, among other things, the geometrical characteristics of the surface of Al-Zn-Sc-Zr alloy samples. He noticed that if the line energy density decreased, the roughness of the top surface increased. In the paper [14], Detwiler et al. analysed the effect of different bulk and contour laser power, scan speed, layer thickness, and build

orientation on the topography of Inconel 718 surfaces produced using the SLM technique. They showed that the surface roughness expressed by deterministic surface topography parameters decreases with increasing layer thickness, but the number of peaks increases with layer thickness because of increased globule formation. Vayssette et al. in their article [15] presented an experimental and numerical approach to investigate the effect of roughness on the fatigue strength of parts additively manufactured from Ti-6Al-4V under high-cycle conditions. They observed that the surface roughness of additively manufactured samples significantly affects their fatigue strength and surface roughness can be reduced by chemical polishing, however, it does not significantly improve fatigue properties. Similar research was conducted by Sanaei and Fatemi [16], according to them the fatigue limit increased with a decrease in surface roughness regardless of the microstructure. In their article [17], Narayanan et al. observed that the surface quality of samples obtained from 18Ni-300 grade maraging steel improves with an increase in the build angle of the samples and as a result of using large pulsed electron-beam (LPEB) irradiation as a post-treatment. Also, a positive effect of finishing on the samples' surface quality was reported by Lesyk et al [18] and Bagehorn et al [32], who additionally showed that there is no direct correlation between a specific roughness value and fatigue life. Studies on the effect of structure direction on the surface macro/microstructure and tribological properties of Inconel 625 samples were also conducted by Yan et al [19]. They showed that the highest roughness value was obtained for the surface produced at an angle of 45°, which they explained by the occurrence of the balling phenomenon and the stair-stepping effect. They obtained the best surface for the 0° plane due to the remelting phenomenon. In their paper, Zakrzewski et al [20] emphasised how the applied process parameters have a significant influence on the quality of the surface obtained as a result of the SLM process. They showed that there is a strong correlation between surface roughness and density, and between the applied volumetric energy density and the obtained density of the samples. The influence of process parameters and the build-up direction of 304L austenitic stainless steel samples on surface quality and fatigue behaviour was studied by Zhang et al [21]. They have shown that the fatigue resistance of horizontal parts is generally

higher than that of vertical parts. Masiagutova et al [22] proved experimentally that there is a relationship between top and side surface roughness and material density, and that roughness is significantly affected by the geometrical arrangement of the melting paths. They also emphasised the compensation and contour roles in shaping the quality of the surfaces obtained. However, Townsend et al [33] reviewed the literature available by 2015 on surface texture metrology in additive manufacturing from metals. They emphasised the role of surface metrology in understanding, improving and optimising manufacturing processes and the appropriate choice of instrumentation as well as measurement scale when characterising surfaces obtained by PBF methods. Similar observations were made in their paper by Thompson et al [34]. Therefore, it can be seen that surface quality measurements in additive processes are of increasing importance, which is likely to become even more important as AM techniques become more widely used as conventional manufacturing processes. Considering the above theorems, it was decided to investigate what effect of the addition of a reinforcing phase, such as TiC, and the angle of the produced surfaces on the surface geometric structure.

EXPERIMENTAL DETAILS

The preparation of samples involved two materials in the form of powder: gas-sprayed H13 tool steel (spherical shape and particle size distribution: $d_{10}=23.84\ \mu\text{m}$, $d_{50}=45.29\ \mu\text{m}$, $d_{90}=142\ \mu\text{m}$ (Fig. 1a)) and nanocrystalline TiC (99+% purity

with a near-spherical shape and a mean particle size of 50 nm (Fig. 1b)). The H13 steel was mixed in a ball mill with TiC, with a concentration of 2.5; 5; 10; 15 % vol. Milling was performed in a high-energy planetary mill (Pulverisette 4, Fritsch GmbH) for 8 hours, using stainless steel balls with a weight ratio to the powder of 5:1. After each 1 hour of milling, the process was stopped for 15 minutes to avoid an excessive rise in temperature inside the grinding bowl. The rotational speed was fixed at 200 rpm. The milling process was performed in the argon atmosphere.

Special samples in accordance with Fig. 2a. were fabricated by the Selective Laser Melting (SLM) additive manufacturing technique. The process was carried out on the REALIZER II 250 (MCP-HEK-Realizer) device equipped with a 100W Nd: YAG laser. The SLM process parameters are summarized in Table 1 – parameters were selected based on previous studies [8].

The above figure also shows the angles at which each surface was produced. Surfaces 1 and 4, and 2 and 3 are parallel (produced at 45° and 30° to the Z-axis respectively) and surface 5 is parallel to the Z-axis. Surfaces 1 and 2 are up-skin surfaces, while 3 and 4 are down-skin surfaces.

In order to compare the compatibility of the 3D model with the real object, a mapping accuracy analysis was performed using a scanning process. Studies on the influence of the reinforcing phase and the angle of inclination of the surface of the obtained samples on selected SGS parameters were performed in the Environmental Measurement Laboratory (EML) of the West Pomeranian University of Technology in Szczecin (ZUT). Measurements were performed using an

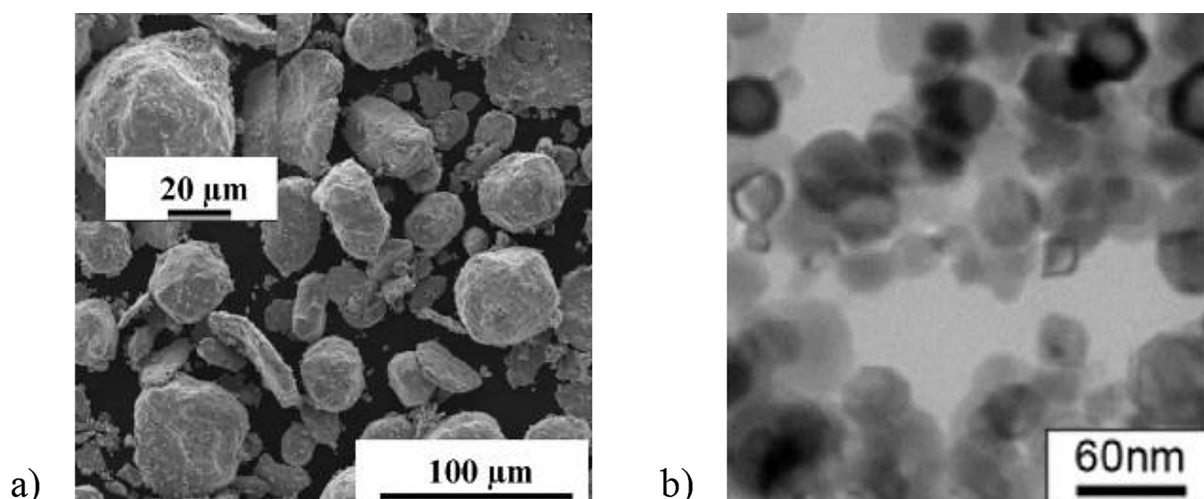


Fig. 1. Microstructures of the starting material: (a) H13 powder, (b) TiC powder

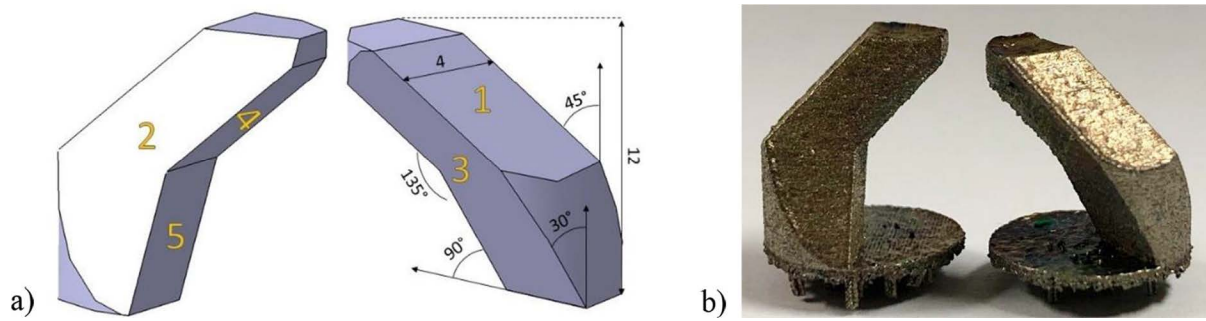


Fig. 2. The geometry of the special samples produced in the SLM process: a) model with marked measurement surfaces and dimensions [mm], b) picture of finished part

Altisurf A520 multisensor surface topography testing machine, from Altimet, equipped with a CL3 chromatic confocal head with an operating range up to 1200 μm and a Z-axis resolution of 22 nm. X-axis drilling was 0.17 μm , Y-axis sampling was 3.00 μm and the measurement field size was 1 mm x 1 mm. The point cloud collected in this way was analysed using AltiMap PREMIUM 6.2 software, then the surface topography was developed in accordance with PN-EN ISO 25178–2:2012. A surface topography analysis methodology was applied to each of the recorded surface point clouds, which included the following procedure:

1. Scanning of the selected surface with digital processing of the point cloud for graphical representation of the measured surface.
2. Setting a threshold value of 0.05–99.95% on each of the extracted measurement fields to remove erroneously collected surface points (deleted points set as unmeasured values).
3. Levelling the surface using the method of least squares.
4. Determination of values of selected stereometric roughness parameters according to ISO 25178.

In this way, two groups of SGP parameters were selected: a) height parameters, which are the basic parameters describing the state of the SGP, b) spatial parameters, which describe features related to the degree of isotropy of the produced surfaces. Among the altitudinal SGS parameters, the following elements were recorded: S_a – arithmetic mean of the surface height, S_z – mean square

deviation of the height of surface irregularities, S_q – mean square deviation of the surface, S_{sk} – surface skewness, S_{ku} – surface kurtosis, S_p – maximum height of the peak, S_y – maximum depth of the valley. They were determined based on spectral analysis of the information contained in the ordinates of the surface in directions consistent with the direction of the X and Y axes of the analysed surface [35].

RESULTS AND DISCUSSION

In the first stage, the accuracy of 3D model representation in the additive manufacturing process was analysed. For this purpose, the samples obtained were scanned using a PICZA LPX 1200 3D Roland scanner equipped with Dr Picza3 software, and then the scans obtained were compared with the initial 3D models. Figure 3 shows the results of the mapping accuracy analysis. The following sample designations were introduced: H13 for a sample made from pure H13 steel, 2.5H13 for a sample made from H13 steel containing 2.5% vol. TiC, 5H13 for a H13 steel sample containing 5% vol. TiC, 10H13 for a H13 steel sample containing 10% vol. TiC and 15H13 for a H13 steel sample containing 15% vol. TiC.

Analysing Figure 3, it can be seen that by far the greater part of the samples obtained were reproduced at a high level. However, as the reinforcing phase increases, the mapping accuracy decreases. The exact deviation values obtained for the individual samples depending on the

Table 1. The selective laser melting process parameters

P [W]	V [mm/s]	h [mm]	d [mm]	E [J/mm ³]
100	250	0.12	0.05	66.667

Note: P – laser power [W], d – layer thickness [mm], h – distance of the laser paths [mm], t – laser exposure time at a single point (s), V – scanning speed [mm/s], E – volumetric energy density [J/mm³].

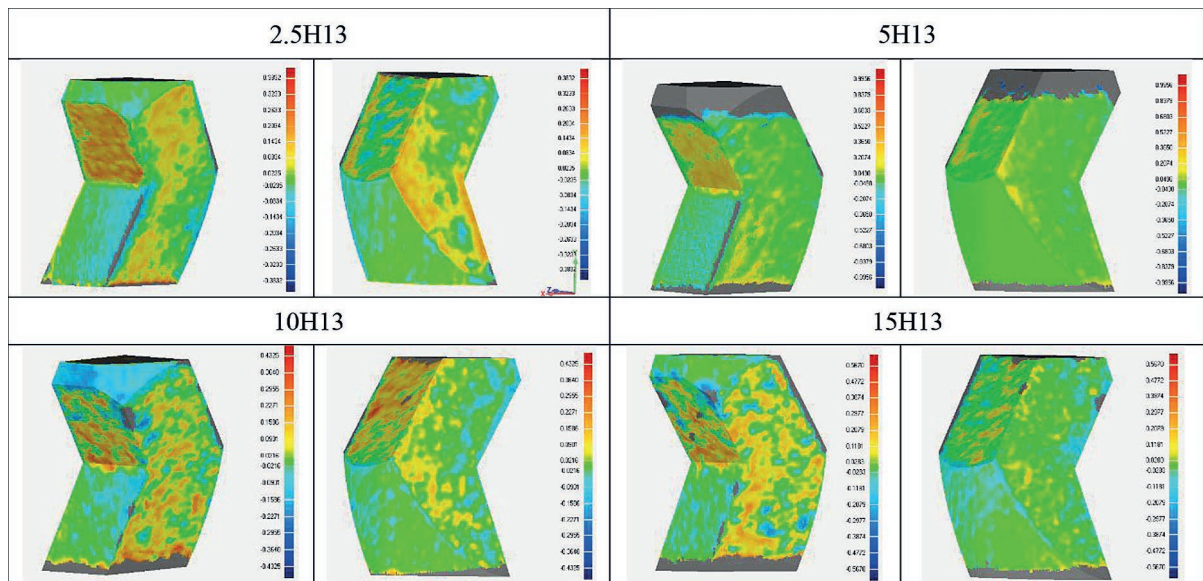


Fig. 3. Results of the model mapping accuracy analysis

proportion of the reinforcing phase are summarised in Table 2.

As the contribution of the reinforcing phase increases, the deviation of the mapping accuracy increases. This is noticeable for both allowance and material loss. The exception to this rule is sample 5H13, for which higher values were obtained than for the sample containing 10% vol. TiC. For the allowance, the values range from 0.3832 mm for 2.5H13 to 0.5670 mm for 15H13. Taking into account the loss of material the deviation values vary from -0.1829 mm for a sample containing 2.5% of TiC vol. to -0.3443 mm for the sample with 15% of TiC content vol. In contrast, the average deviation obtained for the allowance for each sample is quite similar, ranging from 0.0629 to 0.0716 mm. The average deviation obtained for the cavities ranges from -0.0334 for 2.5H13 to 0.1063 for 5H13, with values obtained for the other samples being similar at around -0.04 mm. In the case of standard deviation, the highest value was obtained for sample 5H13 (0.1063 mm), while for the other samples the values obtained were much lower (up to 42%), with the results for samples 10H13 and

15H13 being similar. Similar relationships can be observed for the RMS Estimate. Differences in surface accuracy may be caused, on the one hand, by an uneven distribution of the reinforcing phase in the H13 steel matrix or by the agglomerates produced, and, on the other hand, by the stair-stepping, patterning and balling phenomena occurring during the manufacturing process and the adhesion of partially melted metal powders to the parts produced.

In a further step, SGS measurements were taken. The results of the altitudinal SGS parameters taking into account the contribution of the reinforcing phase and the surface skewness are summarised in Table 3. The numbers of the individual surfaces are as shown in Figure 2.

By analysing the results obtained, it is possible to observe the influence of the reinforcing phase content and the manufacturing angle on the individual parameters. In the case of S_a , it is seen to increase with increasing TiC compactness and build-up angle. The lowest values were obtained for Surface 5 (0° relative to the Z-axis), which is consistent with the publication [19]. According to the literature [16, 17, 19], this parameter

Table 2. The results of model accuracy analysis

Sample variant	Max deviation in + [mm]	Max deviation in - [mm]	Average deviation + [mm]	Average deviation - [mm]	Standard deviation [mm]	RMS Estimate [mm]
2.5 H13	0.3832	-0.1829	0.0629	-0.0334	0.0627	0.0669
5 H13	0.4525	-0.9956	0.0716	-0.0680	0.1063	0.1075
10H13	0.4325	-0.3639	0.0676	-0.0429	0.0753	0.0778
15H13	0.5670	-0.3443	0.0711	-0.0444	0.0791	0.0804

Table 3. Summary of SGP height parameters as a function of reinforcing phase contribution and surface skewness

Sample	$S_a [\mu m]$					$S_z [\mu m]$				
	Surface 1	Surface 2	Surface 3	Surface 4	Surface 5	Surface 1	Surface 2	Surface 3	Surface 4	Surface 5
H13	10.829	9.432	10.750	14.818	8.483	156.335	157.521	184.616	208.800	172.883
2.5H13	30.608	15.119	26.940	0.044	8.452	273.350	139.333	306.236	0.473	174.259
5H13	31.870	24.577	13.037	0.081	16.204	342.852	215.054	126.266	0.703	255.768
10H13	35.602	28.303	0.080	0.078	0.045	370.868	315.143	0.708	0.782	0.482
15H13	0.038	26.947	0.074	0.082	0.043	0.527	335.407	0.648	0.753	0.538
$S_q [\mu m]$						S_{sk}				
Sample	Surface 1	Surface 2	Surface 3	Surface 4	Surface 5	Surface 1	Surface 2	Surface 3	Surface 4	Surface 5
H13	14.258	12.424	14.428	18.630	11.558	0.471	0.409	0.508	0.446	0.289
2.5H13	37.320	18.811	33.994	0.060	12.396	-0.397	0.064	-0.178	-0.729	1.579
5H13	43.775	30.586	17.485	0.101	23.995	1.100	0.057	-0.442	-0.450	2.215
10H13	45.721	35.036	0.106	0.100	0.060	-0.065	-0.265	-0.814	0.012	-1.390
15H13	0.050	37.231	0.092	0.103	0.066	0.886	-0.961	-0.361	0.074	-2.168
S_{ku}						$S_p [\mu m]$				
Sample	Surface 1	Surface 2	Surface 3	Surface 4	Surface 5	Surface 1	Surface 2	Surface 3	Surface 4	Surface 5
H13	4.636	5.083	4.589	3.399	6.361	74.176	80.218	73.204	98.678	69.929
2.5H13	3.170	2.763	3.128	4.197	7.738	108.198	70.101	110.847	0.203	80.742
5H13	4.699	2.831	3.880	3.197	9.557	181.629	104.948	53.242	0.262	159.843
10H13	3.487	3.552	4.036	3.640	5.152	144.591	119.633	0.246	0.356	0.143
15H13	5.810	5.279	3.155	3.153	8.051	0.235	125.196	0.264	0.324	0.167
$S_v [\mu m]$										
Sample	Surface 1	Surface 2	Surface 3	Surface 4	Surface 5					
H13	82.159	77.303	111.412	110.122	102.954					
2.5H13	165.152	69.232	195.389	0.270	93.517					
5H13	161.222	110.106	73.024	0.442	95.925					
10H13	226.276	195.510	0.463	0.427	0.339					
15H13	0.292	210.211	0.385	0.429	0.371					

should be higher for downward-facing surfaces compared to upward-facing surfaces. In this case, however, the results do not fully confirm this relationship. Indeed, for samples in pure H13 steel, the results obtained for down-skin surfaces are worse than for up-skin surfaces (e.g. for Surface 1 – 45° up-skin the recorded S_a value is lower than for Surface 4 – 45° down-skin, similarly with surfaces produced at an angle of 30°). However, in the case of composite materials, the above dependence was not recorded, which could be caused by too large (in relation to the measurement parameters) stair-stepping effect, too many melted powder particles present, uneven distribution of the reinforcing phase or the formation of its agglomerates, which make it impossible to make a correct measurement – especially noticeable at the surface produced at an angle of 45° (Surface 4 down-skin). In order to detail the analysis of the SGS condition, three representative altimetric parameters were selected for further consideration,

i.e. S_q , S_{sk} and S_{ku} . Due to the large power exponent, these last two parameters are very sensitive to sampling and measurement noise. The parameter S_q is determined by an algorithm in the same way as the average effective power of RMS electrical signals (in electronics, this value is used to assess whether a signal is stable and to compare two signals or devices transmitting these signals). In topography analysis, thanks to this value, it is possible to observe how the value of the surface signal S_q changes, it is possible to assess the interference and, in a sense, “lose its power due to surface distortion”. S_{Iz} , anisotropy that characterises physical or geometric properties, was chosen to evaluate the spatial parameters of SGS. Isotropy of SGS means the same surface structure in all directions. At the same time, it is a perfectly symmetrical structure with respect to all possible axes of symmetry [35]. The degree of isotropy is expressed as a percentage ranging from 0% to 100%. By convention, anisotropic surfaces are

assumed to have a degree of isotropy of less than 20%. In contrast, anisotropic surfaces have a degree of isotropy greater than 80%.

Firstly, the effect of the angle of the samples' surface was analysed in terms of the roughness parameters S_q , S_{sk} , S_{ku} and the degree of surface isotropy. Initially, the results obtained for a sample made of pure H13 steel are presented as a reference for further analyses of the influence of the reinforcing phase content on the values of selected SGS parameters. Figure 4 presents the mean square deviation of the roughness – S_q obtained for H13 steel depending on the skewness of the measuring surface.

The surfaces obtained using the SLM method are characterised by a variation of the S_q parameter, which is caused by the layered way of their construction (the “stair-stepping effect” of surfaces not perpendicular and not parallel to the direction of production), variable angles of production of particular surfaces and physical phenomena accompanying the fast melting and cooling of the material in the form of powder (non-uniform size of powder particles, non-uniform shape of the pool of melted material, incompletely melted powder particles). Therefore, when deciding to produce parts by additive methods, it is important to bear in mind that additive techniques cannot exist without further finishing to obtain the appropriate SGS parameters of the mating surfaces [36]. In order to deepen the analysis of the measurement data obtained, Figure 5 shows the summaries of the skewness coefficient S_{sk} and the kurtosis S_{ku} .

Analysing the values of the S_{sk} and S_{ku} parameters, it can be seen that the collected data have a

right-handed asymmetry of distribution, indicating that more data are below the mean S_{sk} value for Surface 1–5. The obtained S_{sk} values (>0) mean the dominance of the peaks comprising the surfaces studied. In addition, when analysing the clustering around the mean value, it can be seen that a significant proportion of the measurement results for Surface 1 – 5 are similar to each other, and there are few data that differ significantly from the mean value.

Figure 6 shows the results of the analysis concerning the degree of surface isotropy for different angles of the produced surface.

Based on Fig. 6, it can be seen that partially melted and agglomerated powders were present on all tested surfaces, which is a characteristic of SLM-produced samples [6]. However, for down-skin surfaces (facing downwards – Surface 3 and 4) there were more of them than on up-skin surfaces (facing upwards – Surface 1 and 2), which is consistent with the literature data in [16, 17]. The reason for these differences is that down-skin surfaces are built on powder with lower thermal conductivity compared to solidified material. This results in less heat dissipation and more particles partially melted and attached to the surface. Another factor is gravity, which causes sagging of unsupported pools of melted layer into unmelted powder [16]. Isotropy analysis has shown that Surface 1 is isotropic – it is structurally symmetric about all possible axes of symmetry. The remaining surfaces, i.e. Surface 2 to 5, have an anisotropic surface. When analysing the depicted degree of isotropy, it is evident that for Surface 3 and 4 it has decreased, which may be due to the angle of surface formation and the direction of build-up

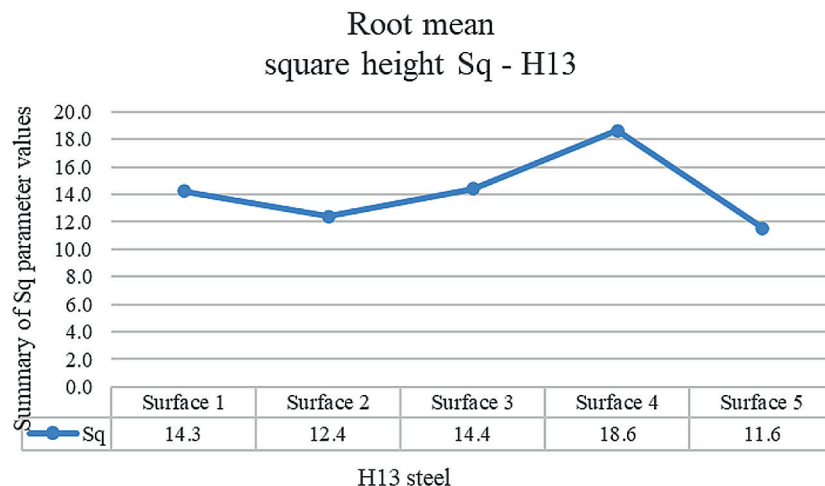


Fig. 4. The chart of the S_q parameter for the H13 steel samples obtained for different measuring surfaces

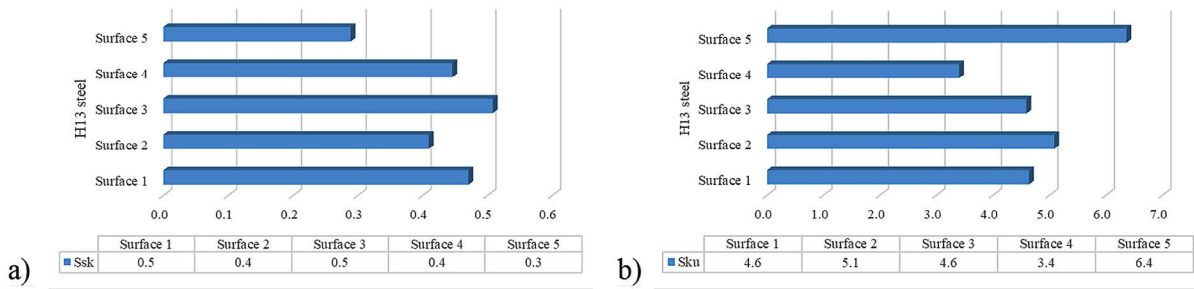


Fig. 5. The chart of parameters a) S_{sk} ; b) S_{ku} for samples made of H13 steel

(these are down-skin surfaces). In order to further analyse the effect of the produced surfaces' angles and the content of the reinforcing phase, it is important to highlight the fact that for samples containing 10 and 15% TiC vol. (Table 2.) it is not possible to analyse the data in detail due to the significant increase in surface roughness and the consequent limitation of the measuring range of confocal sensors. In the case of Surface 2 – 5, it was observed that as the reinforcing phase increases, the parameter S_q increases as well. It is important to highlight the fact that in the case of the Surface 2, the measurement was taken for all prepared planes. In the case of Surface 3 and 5, the value of the S_q parameter was determined for the 2.5 and 5.0 TiC consolidation phase, the other parameters were not determined due to the impossibility of acquisition of the measurement data point cloud. In the case of Surface 4, data for the evaluation of the geometrical structure of the surface were only possible for the pure H13 steel sample. For a consolidation phase content of 2.5 and 5.0% vol, the selected SGS parameters for the different surface angles behaved similarly. Therefore, in the next step, one of the measured surfaces was selected, i.e. Surface 1, to illustrate the effect of the reinforcing phase content on SGS parameters. Figure 7 shows the values of parameter S_q obtained for Surface 1 depending on the share of the reinforcing phase

According to Figure 7, it can be seen that the surface roughness increases with increasing TiC reinforcing phase content (from 14.258 for pure H13 steel to 45.721 for 10 % vol. of TiC content). In the case of a sample containing 15% TiC vol. measurement of the S_q parameter was impossible, due on the one hand to the considerable increase in surface roughness, and on the other to limitations in the capabilities of the chromatic confocal heads in the measurement range (66% of points unmeasured on average for the selected surface). Figure 8 shows the values of parameters S_{sk} , S_{ku}

obtained for Surface 1 depending on the share of the reinforcing phase.

Analysing the values of the S_{sk} and S_{ku} parameters, it can be seen that the collected data have a right-handed asymmetry of distribution, which indicates that more data (for samples H13, 5H13 and 15H13) are below the mean S_{sk} . For samples 2.5H13 and 10H13 there is a left-handed asymmetry of the data distribution, in this case, more data are above the mean value. In addition, by analysing the concentration around the mean value, it can be seen that a significant proportion of the results for all presented TiC reinforcing phases are similar to each other, and there are few data that differ significantly from the mean value. Figure 9 shows the results of the analysis of the degree of surface isotropy obtained for Surface 1 depending on the proportion of the reinforcing phase.

Based on the above results (Fig. 9) for H13 samples and those containing TiC in the range of 2.5% vol., melted powder particles are visible. Similar observations were made by Macek [6]. He observed the presence of unmelted powder particles of H13 steel on fracture surfaces obtained for fatigue test. This indicates the presence of unmelted material particles throughout the specimen. As the proportion of TiC increases, the structure becomes more homogeneous and the unmelted powder particles are less visible. In the range of 10–15% vol. of samples, it can be seen that there are defects such as holes and cracks in the melting area of the powder, which can be caused by the disruption of vapour pockets or by the temperature gradient created between the rapidly heating top surface and the underlying material with relatively slow heat conduction. The expansion of the heated upper layer is limited by the base material. A compressive elastic deformation is induced in the surface layer, which leads to its bending and cracking [17]. Therefore, an increasing proportion of the reinforcing phase may promote cracking. The surface of sample 10H13

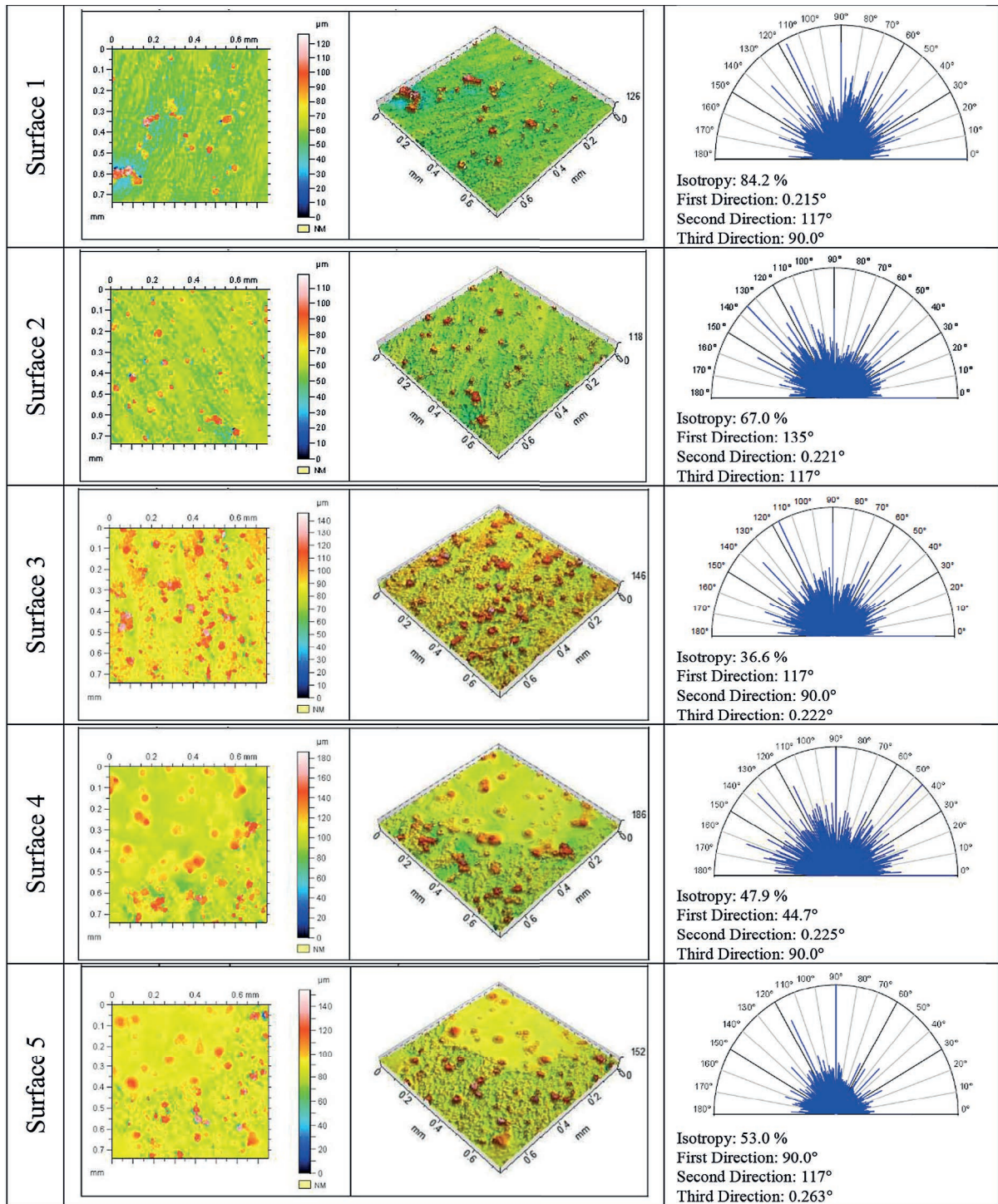


Fig. 6. Summary of the isometric projection and isotropy of the individual surfaces obtained for the H13 steel sample

shows the waviness characteristic of the SLM process due to the movement of the laser beam. The degree of isotropy obtained for Surface 1 for pure H13 steel is 84.2% which indicates that it is isotropic. For samples containing TiC in the range of 2.5–10% vol., the degree of isotropy decreases to about 60%, suggesting that the surfaces obtained for them are mixed anisotropic. An exception to

the above rule is a sample containing 15% vol. of TiC (15H13), for which the degree of isotropy increased and was over 92%. This may be due firstly to hardware limitations, but also with the increase of the proportion of TiC, the structure of the sample becomes more fine and uniform, the surface becomes “flattened” and the symmetry of this shaping increases, i.e. the degree of isotropy

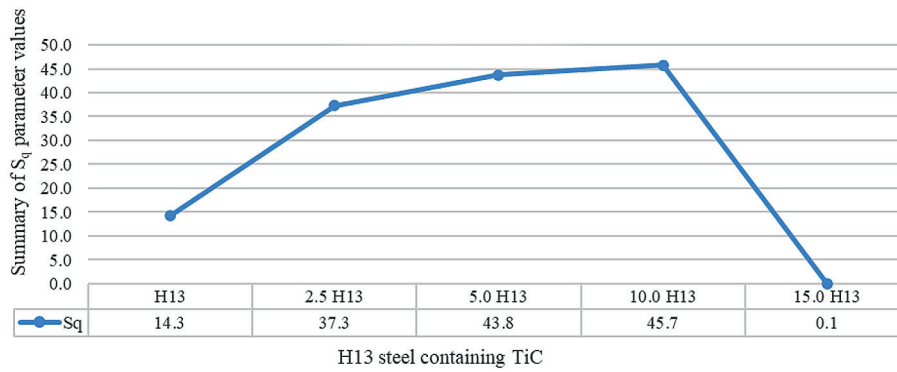


Fig. 7. Summary of S_q parameter values obtained for Surface 1 depending on the proportion of TiC reinforcing phase

increases. The shape of the surface structure, including its degree of isotropy, influences the intensity of wear. Due to the contact between the mating surfaces, which is influenced by the degree of isotropy, the wear can be intermittent or continuous. With a low degree of isotropy (clear directionality), the ridges of the irregularities slide past each other, while with a high degree of isotropy the tops of the micro irregularities rest on each other or hit depressions, furrow the opposite surface or become sheared off. Therefore, functional parameters were used for further analysis in order to check the influence of the reinforcing phase content on the future service life of the component made of H13 steel. Figure 10 shows the Abbott-Firestone curves obtained for Surface 1 depending on the proportion of the reinforcing phase. Functional parameters were also analysed, which are significant tribological parameters and can be used when analysing contact surfaces. They are used to assess the wear resistance of parts, and their analysis is a method used to determine the level of surface defects. In addition, the material share curve was analysed to identify key information about the surface condition affecting the future performance of the component. A

parameter S_{pk} was selected to characterise the upper part of the surface that is most rapidly abraded due to wear, a parameter S_{vk} to assess the ability of sliding surfaces to hold fluid, and a parameter Sk to characterise the effective depth of roughness after a certain period of operation. Its low value may indicate good surface bearing capacity and resistance to high-stress operation.

Based on the results obtained, it can be argued that, depending on the TiC content, a surface that is more or less vulnerable to abrasion can be obtained. By far the best bearing capacity is the surface obtained for composite material 15H13 (15% vol. of TiC), the curve is degressive-progressive, which is important for the future operation of the product. It can be concluded that the S_{pk} for sample 15H13 is small (the parameter value is 0.0965 mm), which indicates the high abrasion resistance of SGS. It can be argued that after the run-in period, there will be no significant changes and the surface will show resistance to wear. It can be seen that as the reinforcing phase increases, the parameter S_{pk} increases which indicates a reduction in quality and durability in future operation. For surfaces that are required to have a high grease holding capacity, the most

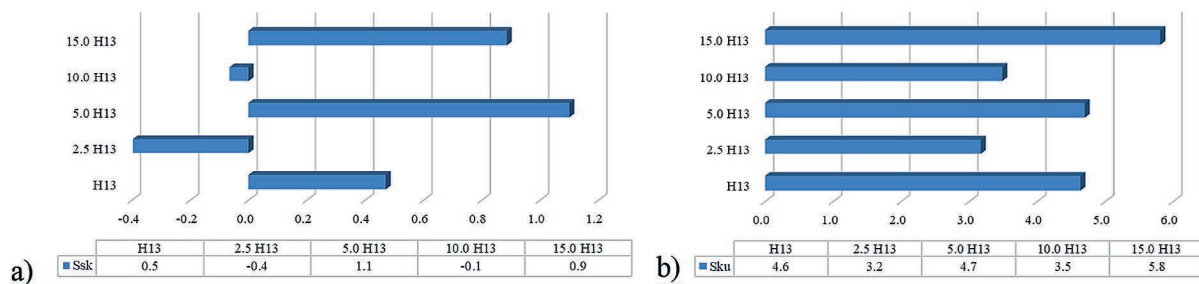


Fig. 8. The chart of S_{sk} and S_{ku} parameters obtained for Surface 1 depending on the proportion of TiC reinforcing phase

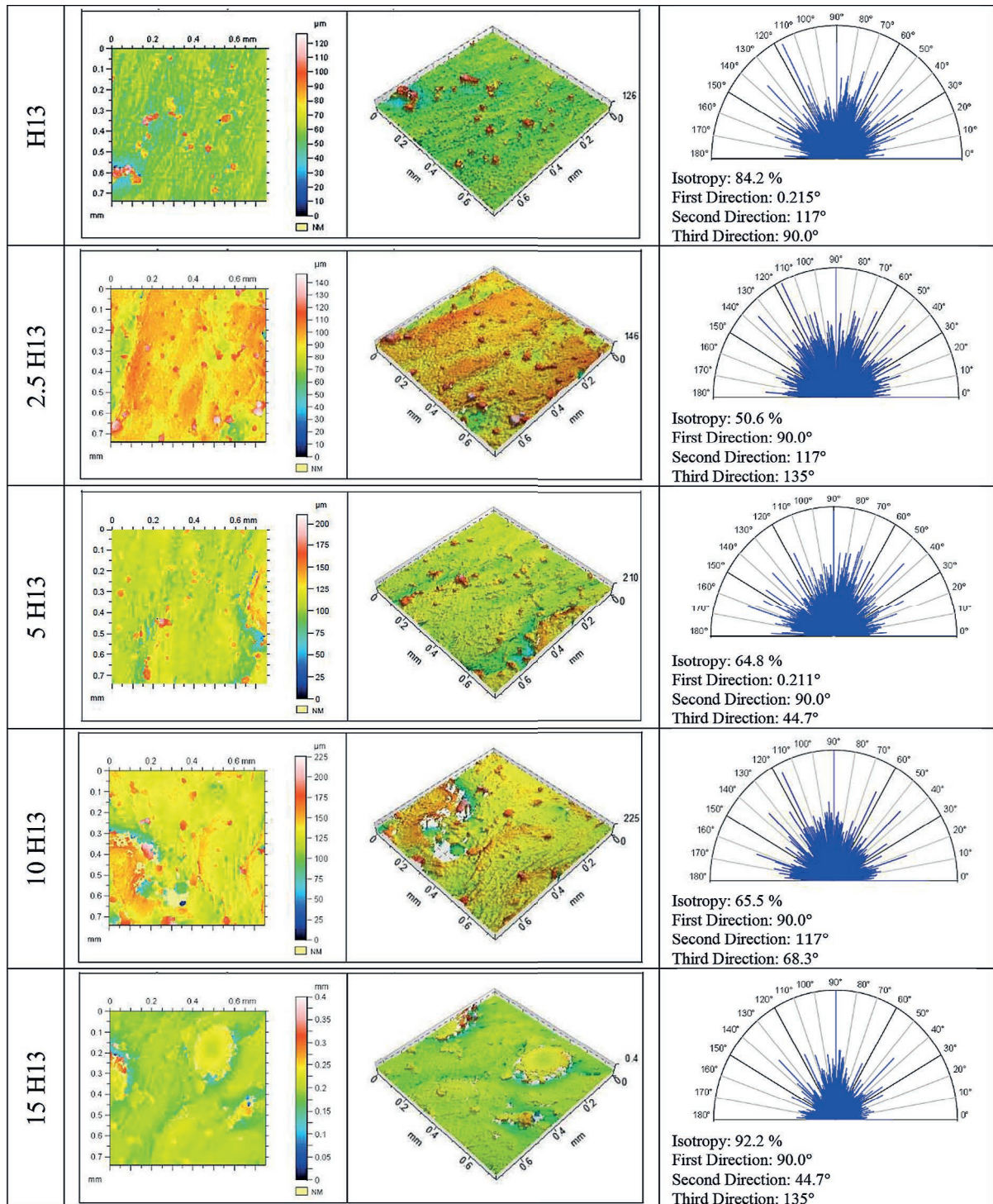


Fig. 9. Summary of the isometric projection and isotropy of Surface 1 depending on the proportion of the reinforcing phase

favourable value of the S_{vk} parameter was obtained for sample 10H13, followed by sample 5H13. In the case of a sample containing 10% of TiC vol. is the most favourable from the point of view of resistance to the transmission of contact loads and surface abrasiveness when interacting with another surface.

CONCLUSIONS

In the present work, the influence of the surface angle and the content of the nano TiC reinforcing phase on the geometric structure of the H13 steel surface obtained by selective laser melting was studied. The geometric structure

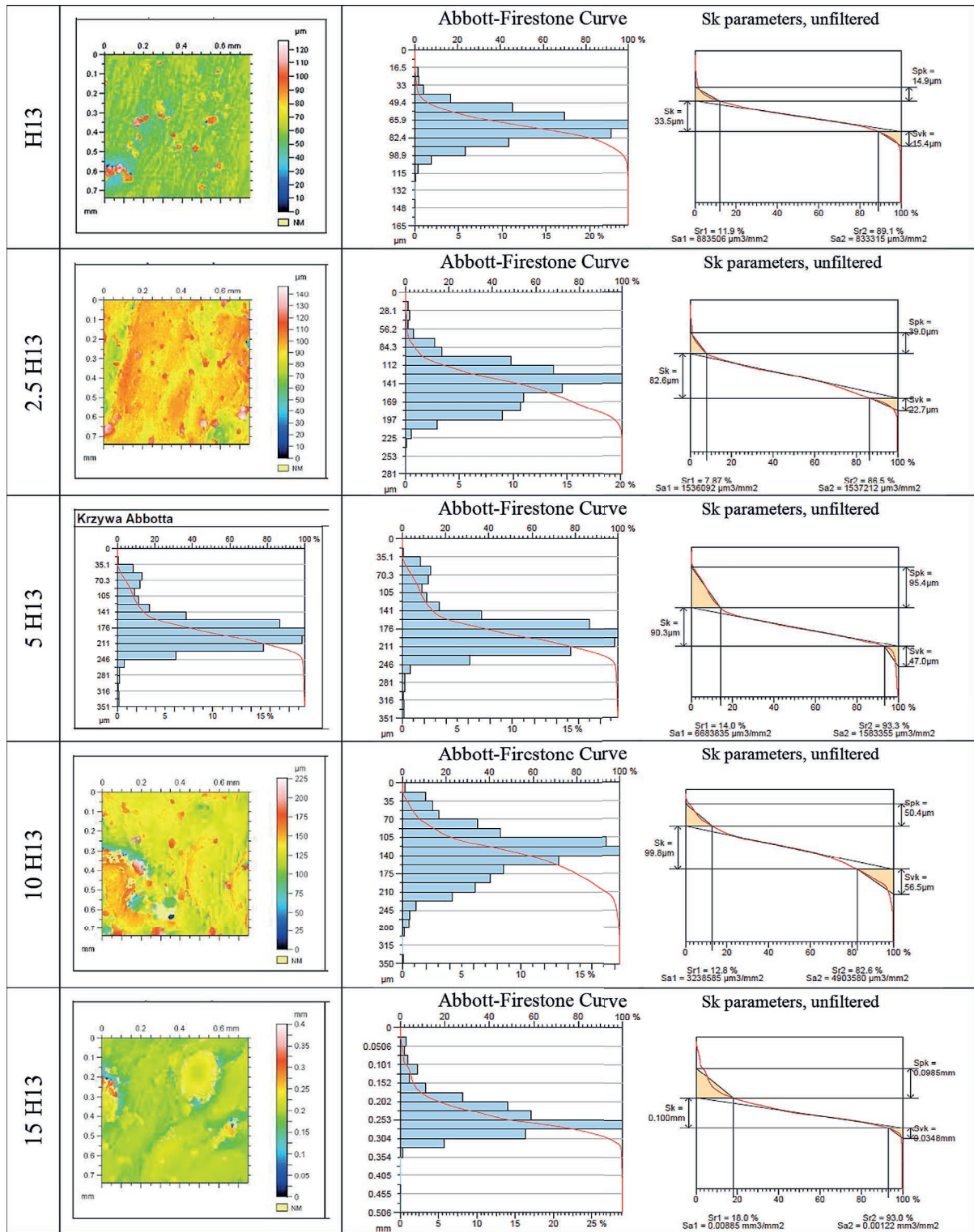


Fig. 10. Summary of the Abbott-Firestone curve of Surface 1 depending on the proportion of the reinforcing phase

of the surface measurements made it possible to draw the following conclusions. For samples containing at least 10% by vol. partially melted powder particles and agglomerates were found on the surface, as well as cracks and pores. No waviness was observed for most of the studied

surfaces (sample 10H13 is an exception). The resulting surface quality was better for upward-facing than downward-facing produced at the same angle. The surface quality of the samples deteriorated as the build-up angle increased (from 30° to 45°) for the up-skin surface. In the case

of down-skin surfaces, the results obtained are not unambiguous and cannot support the above thesis due to problems with data recording by the measuring apparatus, which could be caused by the occurrence of stair-stepping, patterning, and balling phenomena characteristic for the SLM process, as well as the adhesion of partially melted metal powders to the produced elements (e.g. Surface 4). The best surface quality was recorded for the 0° surface which is related to the remelting phenomenon. As the proportion of the reinforcing phase increased, a deterioration in surface quality was observed, with the measuring apparatus having problems reading the data for higher contents (>10% vol.). Furthermore, a deterioration in the quality of the model representation was noted as the proportion of the reinforcing phase increased.

The research carried out allows us to claim that by using selected production angles and surface orientation (downward or upward), as well as the appropriate content of the reinforcing phase, it is possible to obtain surfaces characterised by different SGS quality, and thus the SGS properties can be planned accordingly.

Acknowledgements

We thank Dariusz Grzesiak, PhD (West Pomeranian University of Technology, Szczecin) for assistance with samples and for comments that greatly improved the manuscript.

REFERENCES

1. Dadoo A., Boutorabi S.M.A., Kheirandish S. Effect of titanium carbide concentration on the morphology of MC carbides. *Optics and Laser Technology* 2019; 112: 236–244.
2. Dadoo A., Boutorabi S.M.A. Correlation between pulsed laser parameters and MC carbide morphology in H13 tool steel/TiC composite coating. *Optics and Laser Technology* 2020; 127: 106120.
3. Chen H., Lu Y., Sun Y., Wei Y., Wang X., Liu D. Coarse TiC particles reinforced H13 steel matrix composites produced by laser cladding. *Surface & Coatings Technology* 2020; 395: 125867.
4. Kazemi M., Saghafian H. Application of response surface methodology in determining the optimal wear properties of the titanium carbide reinforced AISI H13 hot working tool steel fabricated by pulsed laser method. *Surface & Coatings Technology* 2020; 404: 126478.
5. Henschel S., Kietov V., Deirmina F., Pellizzari M., Krüger L. Fracture toughness of a hot work tool steel-TiC composite produced by mechanical milling and spark plasma sintering. *Materials Science & Engineering A* 2018; 709: 152–159.
6. Macek W., Martins R.F., Branco R., Marciniak Z., Szala M., Wroński S. Fatigue fracture morphology of AISI H13 steel obtained by additive manufacturing. *International Journal of Fracture* 2022; 235: 79–98.
7. Meng Ch., Cao R., Li J., Geng F., Zhang Y., Wu Ch., Wang X., Zhuang W. Mechanical properties of TiC-reinforced H13 steel by bionic laser treatment. *Optics & Laser Technology* 2021; 136: 106815.
8. Al Mangour B., Grzesiak D., Yang J-M. Nanocrystalline TiC-reinforced H13 steel matrix nanocomposites fabricated by selective laser melting. *Materials and Design* 2016; 96: 150–161.
9. AlMangour B., Grzesiak D., Yang J-M. Selective laser melting of TiB2/H13 steel nanocomposites: Influence of hot isostatic pressing post-treatment. *Journal of Materials Processing Technology* 2017; 244: 344–353.
10. Fedrizzi A., Pellizzari M., Zadra M., Marin E. Microstructural study and densification analysis of hot work tool steel matrix composites reinforced with TiB2 particles. *Materials Characterization* 2013; 86: 69–79.
11. Hamed M.J., Torkamany M.J., Sabbaghzadeh J. Effect of pulsed laser parameters on in-situ TiC synthesis in laser surface treatment. *Optics and Lasers in Engineering* 2011; 49(4): 557–563.
12. Shuming Z., Xianfeng S., Jialin Y., Wenhua T., Yingying W. Densification behavior and mechanical properties of nanocrystalline TiC reinforced 316L stainless steel composite parts fabricated by selective laser melting. *Optics and Laser Technology* 2018; 103: 239–250.
13. Bi J., Zhenglong L., Yanbin Ch., Xi Ch., Xikun Q., Ze T. Effect of Process Parameters on Formability and Surface Quality of Selective Laser Melted Al-Zn-Sc-Zr Alloy from Single Track to Block Specimen. *Optics & Laser Technology* 2019; 118: 132–39.
14. Sean D., Watring D., Spear A., Raeymaekers B. Relating the Surface Topography of As-Built Inconel 718 Surfaces to Laser Powder Bed Fusion Process Parameters Using Multivariate Regression Analysis. *Precision Engineering* 2022; 74: 303–15.
15. Bastien V., Saintier N., Brugger Ch., El May M. Surface Roughness Effect of SLM and EBM Ti-6Al-4V on Multiaxial High Cycle Fatigue. *Theoretical and Applied Fracture Mechanics* 2020; 108: 102581.
16. Niloofar S., Fatemi A. Analysis of the Effect of Surface Roughness on Fatigue Performance of Powder Bed Fusion Additive Manufactured Met-

- als. Theoretical and Applied Fracture Mechanics 2020; 108: 102638.
17. Sankara Narayanan T.S.N., Kim J., Jeong H.E., Park H.W. Enhancement of the Surface Properties of Selective Laser Melted Maraging Steel by Large Pulsed Electron-Beam Irradiation. Additive Manufacturing 2020; 33: 101125.
 18. Lesyk D. A., Martinez S., Mordyuk B. N., Dzhemelinskyi V. V., Lamikiz A., Prokopenko G. I. Post-Processing of the Inconel 718 Alloy Parts Fabricated by Selective Laser Melting: Effects of Mechanical Surface Treatments on Surface Topography, Porosity, Hardness and Residual Stress. Surface and Coatings Technology 2020; 381: 125136.
 19. Xingchen Y., Shuohong G., Cheng Ch., Jian H., Khashayar K., Dongdong D., Wenyong M., Nouredine F., Hanlin L., Min L. Effect of Building Directions on the Surface Roughness, Microstructure, and Tribological Properties of Selective Laser Melted Inconel 625. Journal of Materials Processing Technology 2021; 288: 116878.
 20. Zakrzewski, T., Kozak J., Witt M., Dębowska-Wąsac M. Dimensional Analysis of the Effect of SLM Parameters on Surface Roughness and Material Density. Procedia CIRP 2020; 95: 115–20.
 21. Zhang, Hongzhuang, Mengtao Xu, Zhendong Liu, Changyou Li, Punit Kumar, Zhenhua Liu, i Yimin Zhang. „Microstructure, Surface Quality, Residual Stress, Fatigue Behavior and Damage Mechanisms of Selective Laser Melted 304L Stainless Steel Considering Building Direction”. Additive Manufacturing 2021; 46: 102147.
 22. Masiagutova E., Cabanettes F., Sova A., Cici M., Bidron G., Bertrand P. Side Surface Topography Generation during Laser Powder Bed Fusion of AlSi10Mg. Additive Manufacturing 2021; 47: 102230.
 23. Zhang M., Li C., Gao Q., Fang J., Wu T. L., Wang K. H. The effect of heat treatment on microstructure and properties of laser-deposited TiC reinforced H13 steel matrix composites. Optik – International Journal for Light and Electron Optics 2020; 206: 164286.
 24. Gu S. T., Chai G. Z., Wu H. P., Bao Y. M. Characterization of local mechanical properties of laser-cladding H13–TiC composite coatings using nanoindentation and finite element analysis. Materials and Design 2012; 39: 72–80.
 25. Novichenko D., Marants A., Thivillon L., Bertrand Ph., Smurov I. Metal Matrix Composite Material by Direct Metal Deposition. Physics Procedia 2011; 12: 296–302.
 26. Szymanski Ł., Olejnik E., Sobczak J., Szala M., Kurtyka P., Tokarski T., Janas, A. Dry sliding, slurry abrasion and cavitation erosion of composite layers reinforced by TiC fabricated in situ in cast steel and gray cast iron. Journal of Materials Processing Tech. 2022; 308:117688
 27. Olejnik E., Szymański Ł., Batóg P., Tokarski T., Kurtyka P. TiC-FeCr local composite reinforcements obtained in situ in steel casting Journal of Materials Processing Technology 2003; 277: 1–9.
 28. Janicki, D. Microstructure and Sliding Wear Behaviour of In-Situ TiC-Reinforced Composite Surface Layers Fabricated on Ductile Cast Iron by Laser Alloying. Materials 2018; 11: 75.
 29. Chinmaya K. S., Manoj M., Effect of pulse laser parameters on TiC reinforced AISI 304 stainless steel composite coating by laser surface engineering process. Optics and Lasers in Engineering 2015; 67: 36–48.
 30. Sahoo C.K., Masanta M. Effect of pulse laser parameters on TiC reinforced AISI 304 stainless steel composite coating by laser surface engineering process. Optics and Lasers in Engineering 2015; 67: 36–48.
 31. Wei P., Wei Z., Zhen Ch., Du J., He Y., Li J., Zhou Y. The AlSi10Mg Samples Produced by Selective Laser Melting: Single Track, Densification, Microstructure and Mechanical Behavior. Applied Surface Science 2017; 408: 38–50.
 32. Bagehorn, S., Wehr J., Maier H. J. Application of Mechanical Surface Finishing Processes for Roughness Reduction and Fatigue Improvement of Additively Manufactured Ti-6Al-4V Parts. International Journal of Fatigue 2017; 102: 135–42.
 33. Townsend, A., Senin N., Blunt L., Leach R. K., Taylor J. S. Surface Texture Metrology for Metal Additive Manufacturing: A Review. Precision Engineering 2016; 46: 34–47.
 34. Thompson A., Senin N., Giusca C, Leach R. Topography of Selectively Laser Melted Surfaces: A Comparison of Different Measurement Methods. CIRP Annals – Manufacturing Technology 2017; 66(1): 543–46.
 35. Bachtiaik-Radka E., Grochała D., Chmielewski K., Olszak W. Isotropy tests of milled and burnished steel surfaces X160CRMOV121. Mechanik 2015; 88(8–9): 641–653.
 36. Królikowski M., Krawczyk M. Does Metal Additive Manufacturing in Industry 4.0 Reinforce the Role of Subtractive Machining? Advances in Manufacturing II edited by Justyna Trojanowska, Olaf Ciszak, José Mendes Machado, i Ivan Pavlenko, 150–64. Lecture Notes in Mechanical Engineering. Cham: Springer International Publishing, 2019.